

# PCCP

Accepted Manuscript



This is an *Accepted Manuscript*, which has been through the Royal Society of Chemistry peer review process and has been accepted for publication.

*Accepted Manuscripts* are published online shortly after acceptance, before technical editing, formatting and proof reading. Using this free service, authors can make their results available to the community, in citable form, before we publish the edited article. We will replace this *Accepted Manuscript* with the edited and formatted *Advance Article* as soon as it is available.

You can find more information about *Accepted Manuscripts* in the [Information for Authors](#).

Please note that technical editing may introduce minor changes to the text and/or graphics, which may alter content. The journal's standard [Terms & Conditions](#) and the [Ethical guidelines](#) still apply. In no event shall the Royal Society of Chemistry be held responsible for any errors or omissions in this *Accepted Manuscript* or any consequences arising from the use of any information it contains.



Journal Name

ARTICLE

Received 00th January 20xx,  
Accepted 00th January 20xx

DOI: 10.1039/x0xx00000x

www.rsc.org/

## Molecular Dynamics Study of di-CF<sub>4</sub> Based Reverse Micelle in Supercritical CO<sub>2</sub>

Bing Liu<sup>a,b,\*</sup>, Xinpeng Tang<sup>a</sup>, Wenjing Fang<sup>a</sup>, Xiaoqi Li<sup>a</sup>, Jun Zhang<sup>a</sup>, Zhiliang Zhang<sup>b</sup>, Yue Shen<sup>a</sup>,  
Youguo Yan<sup>a</sup>, Xiaoli Sun<sup>a</sup>, Jianying He<sup>b,\*</sup>

The reverse micelles (RMs) in supercritical CO<sub>2</sub> (scCO<sub>2</sub>) are promising alternatives for organic solvents, especially for both polar and non-polar components are involved. Fluorinated surfactants, particularly the double-chain fluorocarbon surfactants, are appropriate to form well-structured RMs in scCO<sub>2</sub>. The mechanisms inherent to the self-assembly of the surfactants in scCO<sub>2</sub> are still subject to discussion. In this study, molecular dynamics simulations were performed to investigate the self-aggregation behavior of di-CF<sub>4</sub> based RM in scCO<sub>2</sub> and a stable and spherical RM is formed. The dynamics process and the self-assembly structure in the RM reveal a three-step mechanism to form the RM, that is, small RMs, rod-like RMs and the fusion of rod-like RMs. The Hydrogen-bonds between headgroups and water molecules, and the salt bridges linking Na<sup>+</sup>, headgroups and water molecules enhance the interfacial packing efficiency of the surfactant. The result shows the di-CF<sub>4</sub> molecule has the high surfactant coverage at the RM interface, implying the high CO<sub>2</sub>-philicity. This mainly results from the bend of the short chain (C-COO-CH<sub>2</sub>-(CF<sub>2</sub>)<sub>3</sub>-CF<sub>3</sub>) due to the flexible carboxyl group. The microscopic insight provides in this study is helpful to understand the surfactant self-assembly phenomena and design new CO<sub>2</sub>-philic surfactants.

### 1. Introduction

Supercritical CO<sub>2</sub> (scCO<sub>2</sub>) has been considered as an ideal green replacement for organic solvents owing to its favourable chemical properties, such as nontoxic, non-flammable, environmental benignity and potentially recyclable<sup>1-4</sup>. However, neat scCO<sub>2</sub> can only dissolve nonpolar and small molecular mass materials, with common polar or high molecular mass materials always separating from dense scCO<sub>2</sub><sup>5</sup>. Such limitations obviously restrict many potential applications of scCO<sub>2</sub>. A massive efforts have been made into the design of CO<sub>2</sub>-philic surfactants to improve solvency characteristics of scCO<sub>2</sub>. Formation of water-in-CO<sub>2</sub> (w/c) reverse micelles (RMs) or microemulsions has been widely accepted as a promising approach to improve the solubilising power of scCO<sub>2</sub>. The w/c reverse micelle is the surfactant aggregate in CO<sub>2</sub> continuum and contains a water nanodroplet

in the micellar core. The interior water domain enhances the solubility of solutes which are insoluble in CO<sub>2</sub>. Because the w/c RMs have attractive properties of scCO<sub>2</sub>, as well as the solvation properties of water, they have the potential as volatile organic compound (VOC)-free and energy-efficient solvents for nanomaterial synthesis, enzymatic reactions, dry-cleaning, dyeing, preparation of inorganic/ organic hybrid materials, and so on<sup>6-8</sup>.

To date, the most successful CO<sub>2</sub>-philic surfactants are fluorocarbon-based surfactants due to their high solubility of fluorocarbon chains in scCO<sub>2</sub><sup>9-15</sup>. These surfactants can be solubilised in scCO<sub>2</sub> to form w/c reverse micelles. Among these surfactants, the anionic di-fluorocarbon chain surfactant, [Na][di-CF<sub>4</sub>] (sodium bis-(1-H, 1-H-perfluoropentyl)-2-sulfosuccinate), exhibits the optimum molecular structure<sup>16</sup>, the low fractional free volume (FFV), the low phase-transition pressure, and the high relative surfactant coverage ( $\Phi_{\text{surf}}$ ) of any known CO<sub>2</sub>-philic surfactant<sup>17</sup>. These advantages render it the most efficient reverse micelle stabilizer.

Numerous experimental studies have been performed to elucidate how tail and headgroup structure as well as surfactant counterions influence the self-assembly properties of surfactants in scCO<sub>2</sub><sup>1, 4, 17-19</sup>. The results showed that the chain length and fluorination at the terminal carbon atoms are

<sup>a</sup> School of Science, China University of Petroleum, Qingdao 266580, Shandong, China.

<sup>b</sup> NTNU Nanomechanical Lab, Department of Structural Engineering, Norwegian University of Science and Technology (NTNU), Trondheim, 7491, Norway.

\* Corresponding authors:

Email: [liubing19720115@gmail.com](mailto:liubing19720115@gmail.com); [jianying.he@ntnu.no](mailto:jianying.he@ntnu.no)

Electronic Supplementary Information (ESI) available: [di-CF<sub>4</sub> surfactant molecular formula; details of CHARMM-27 forcefield potential function; parameters for molecules used in this work; a final structure of a larger system; details of the calculating method of the surfactant coverage]. See DOI: 10.1039/x0xx00000x

crucial factors for surfactants to effectively stabilize w/c microemulsions<sup>20</sup>; the FFV and  $\Phi_{\text{surf}}$  at the water-CO<sub>2</sub> interface are important parameters affecting CO<sub>2</sub>-philicity<sup>17</sup>; and the hydration radius and the valence of counterion play an important role in shape and stability of w/c microemulsions<sup>19</sup>. Experimental techniques involving NMR, small-angle neutron scattering (SANS) and X-ray scattering have been employed to characterize surface/interface properties and shapes of w/c RMs. Although previous experiments have provided extensive information, the microscopic self-assembly process and the detailed RMs structure information at high pressure condition have not yet to be convincingly elucidated.

On the other hand, molecular dynamics (MD) simulations have been applied to demonstrate the entire process of self-aggregation and the RM structure even in atomic scale. Salaniwal et al. reported a two-steps mechanism to the RM formation<sup>17</sup>. Zhuo et al. speculated a four-steps mechanism to a CO<sub>2</sub>-induced microstructure transition of the lamellar bilayer using MD simulation<sup>21</sup>. Lu and Berkowitz showed a successful aggregation of a RM and concluded that the fluorinated surfactants are effective in creating w/c RMs<sup>22</sup>. Berkowitz et al. studied the effect of the counterions (NH<sub>4</sub><sup>+</sup>, Na<sup>+</sup>, Ca<sup>2+</sup>) in surfactant PFPE on the structural and dynamical properties of water in RMs. Their results showed that the bridges connecting ions and charged headgroups display long orientational relaxation time. Yuan et al. found three types of salt bridges shielding the electrostatic repulsion between polar headgroups in surfactant monolayer on the water surface. In early studies, the hydrogen bonds formed between headgroups and water were regarded as one of the driving force in a w/c RM<sup>18</sup>. Tamsamani et al.<sup>23</sup> found that water-headgroup hydrogen bonds increased with the increase of  $W_0$ . However, for a given  $W_0$ , the counterion size has only a small effect on the extent of water-headgroup hydrogen bonds. Faeder et al.<sup>24</sup> reported that the water-headgroup hydrogen bonds decrease in a water-in-oil RMs system upon exchanging Na<sup>+</sup> with K<sup>+</sup>. Rossky et al.<sup>25-28</sup> investigated the FFV on a planar water-CO<sub>2</sub> interface and reported that a high  $\Phi_{\text{surf}}$  can improve the CO<sub>2</sub>-philicity of a given surfactant. However, the mechanisms inherent to the self-assembly of the surfactant in scCO<sub>2</sub> are still not well understood. Thus, it could be interesting to have an insight on the RM behaviour of surfactant di-CF<sub>4</sub> in scCO<sub>2</sub>, the counterion effect on the RM, and the intrinsic relation between  $\Phi_{\text{surf}}$  and the tailgroups.

In this work, molecular dynamics simulations were carried out to investigate the fundamental mechanism of the self-assembly in the water/di-CF<sub>4</sub>/scCO<sub>2</sub> system at the atomic level. Firstly, we investigated the dynamics process in the RMs to understand the self-assembly behaviour. Then, we calculated the radial density profiles for the species in the system as well as the time evolution of the radius of gyration to study the structure of the RM. In addition, we analysed the

hydrogen bonds and salt bridges in the RM to describe the binding behaviour among the surfactant, water and counterions. Finally, we computed the  $\Phi_{\text{surf}}$  over the spherical RM interface and illustrated the relation between  $\Phi_{\text{surf}}$  and the change in the tailgroups of the di-CF<sub>4</sub> molecule. Understanding the mechanism of the surfactant self-assembly in scCO<sub>2</sub> phase is beneficial not only to gain insight into the self-assembly phenomena but also to design new type of CO<sub>2</sub>-philic surfactants.

## 2. Simulation Details

The CHARMM-27 force field<sup>29-31</sup> was used for the [Na][di-CF<sub>4</sub>] molecules whose parameters were generated by the swissparam software<sup>32</sup>. The swissparam software is a professional producer for small organic molecules in CHARMM-27 force field using in GROMACS. The classical SPC/E model<sup>33</sup> was employed to describe water molecules. The CO<sub>2</sub> molecules was described by the three-site EPM2 model<sup>34</sup> which can accurately reproduce the experimental critical point and liquid-vapour coexistence curve. The cross terms for non-like components were obtained through Lorentz-Berthelot mixing rules<sup>35, 36</sup>. All force field parameters for various components in the system we studied were given in Electronic Supplementary Information (ESI).

We performed MD simulations on a three-component mixture composed of surfactants ([Na][di-CF<sub>4</sub>]), scCO<sub>2</sub> and water. Initially, we randomly put 4000 CO<sub>2</sub> molecules, 25 surfactants and 125 water molecules with  $W_0=5$  ( $W_0=[\text{water}]/[\text{surfactant}]$ ) in a 6\*6\*6 nm<sup>3</sup> box where the density is close to the real density of the complicated system. In order to get a reasonable density of the three-component system, we run a MD simulation for 2 ns in NPT ensemble under 313 K and 40 MPa. After the simulation the box size changes to 6.8\*6.8\*6.8 nm<sup>3</sup>. Then under the same conditions, we rebuilt a new system as the initial model which was set to be 6.8\*6.8\*6.8 nm<sup>3</sup> using a smart software package packmol<sup>37</sup>, shown in Fig 1 (a). To investigate the microscopic process of the self-aggregation of di-CF<sub>4</sub> in scCO<sub>2</sub>, we carried out a MD simulation for 30 ns in NVT ensemble. To eliminate the occasionality of the result, 5 MD simulations were run under the same conditions. To get a clear spherical shape of the RM and improve the simulation efficiency, in this study, we choose  $W_0=5$  instead of  $W_0=10$  used in the experiment<sup>38</sup>. The final configuration for  $W_0=10$  was presented in ESI. In addition, we performed a MD simulation on a larger system with 100 di-CF<sub>4</sub> molecules and 500 water molecules to eliminate the aggregation process difference caused by the number of the surfactants (see in ESI).

All MD simulations were performed using the GROMACS free software package (version 4.5.5)<sup>39</sup>. And the visualization of the dynamics process using the program VMD<sup>40</sup>. The initial

configurations were minimized by the steepest decent methods. When the maximum force of the system was converged to a threshold of less than  $1000 \text{ kJ}\cdot\text{mol}^{-1}\cdot\text{nm}^{-1}$ , the whole energy of the system was considered to be low enough to perform a dynamics simulation. The temperature of the system was kept 313 K by nose-hoover thermostat algorithm with a coupling constant of 0.2 ps<sup>41, 42</sup>. The nonbonded potential truncation was performed with a cut-off distance at 1.0 nm for Lennard-Jones potential<sup>43</sup>. The long-range part of the electrostatic interactions was treated by the particle mesh Ewald method (PME)<sup>44</sup>. The time step of NVT or NPT simulation was set to 1 fs. Periodic boundary condition were employed in all three directions. The Maxwell–Boltzmann distribution was employed to set the initial atomic velocities of the system<sup>45</sup>. The trajectories were collected in an interval of 1 ps. After the 30 ns simulation, another 2 ns simulation was performed to collect data used for further analysis.

### 3. Results and Discussion

#### 3.1 Self-assembly Process

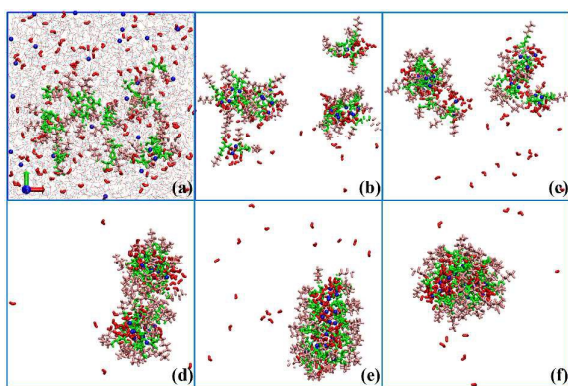


Fig. 1. Time evolution of the ternary mixture of [Na][di-CF<sub>4</sub>]/water/CO<sub>2</sub> at  $W_0 = 5$ . Snapshots are taken at (a) 0 ns (b) 0.2 ns (c) 0.45 ns (d) 14 ns (e) 16 ns (f) 30 ns. Color scheme: green = surfactants headgroups; pink = surfactants tailgroups; red = water; blue = sodium. In (b)-(f), scCO<sub>2</sub> are not shown for clarity.

To visualize self-assembly behaviour of the RM in a three-component system containing scCO<sub>2</sub>, [Na] [di-CF<sub>4</sub>], and water starting from a random configuration, a series of snapshots, illustrating the evolution of the system from the initial configuration to a spherically shaped RM configuration, were provided in Fig. 1. From the simulation, it is observed that water molecules and di-CF<sub>4</sub> molecules aggregate and form several scattered small RMs during very short simulation time of 0.2 ns, shown in Fig. 1(b). Further these small aggregates cluster into two larger RMs at about 0.45 ns, shown in Fig. 1(c). The two aggregates exist for a long simulation time with the structure relaxation, shown in Fig. 1(d). During this process,

although the two aggregates contact many times, they do not merge into one bigger RM yet because of the weaker interaction between the surfactants fluorinated tailgroups. The water core in each aggregate is not completely parcelled by surfactants and a small part of the outer surface of the water core is bare. At 14.0 ns, the two aggregates contact each other via the bare parts of water cores. Because the two water cores contact, the two aggregates merge into an unstable rod-like RM at about 16.0 ns, shown in Fig. 1(e). Beyond this time, the unstable rod-like aggregates rearranges its structure through the strong water-water cohesive interaction. The water core shrinks to a stable spherical droplet and the stable RM is finally formed, as shown in Fig. 1(f). Moreover, the presence of water cores provides a medium screening effect, which attenuates the electrostatic repulsion between head groups of the surfactants. It facilitates the fusion process in which two aggregates merge into one large reverse micelle. This dynamical process for the di-CF<sub>4</sub> self-assembly in the water-in CO<sub>2</sub> microemulsion is qualitatively similar with the previous report in the water/surfactant/CO<sub>2</sub> system<sup>5, 6, 22, 46</sup>. The percolation threshold could not occur in the system due to the low volume fraction (0.065) of water plus surfactants<sup>47, 48</sup>.

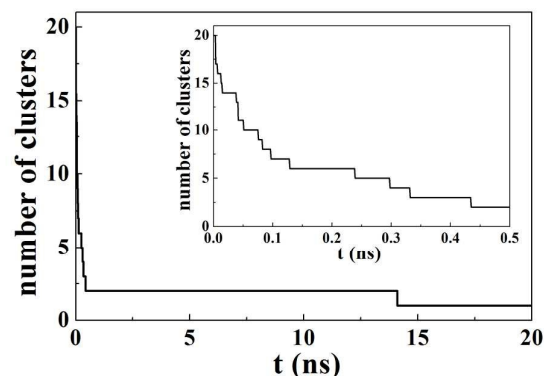


Fig. 2. Evolution of the number of aggregates in the water/di-CF<sub>4</sub>/scCO<sub>2</sub> system during the course of simulation.

To depict the rapid micellization followed by a relatively long period of stabilization of the clusters, the number of aggregates existing during the course of the simulation was plotted in Fig. 2. An aggregate is determined by the single-linkage method<sup>49</sup> with a root mean square deviation (RMSD) cutoff distance of 0.1 nm. It is observed that there are three stages occurring in the self-assembly process of water/di-CF<sub>4</sub>/scCO<sub>2</sub> system. The number of aggregates decreases rapidly from 20 to 2 before 0.5 ns, clearly shown in the inset. During this process, the system containing 6 or 3 aggregates remains for a longer time than others, which means the aggregates with 4 or 8 di-CF<sub>4</sub> molecules is more stable. From 0.5 ns to 14.5 ns, the number of aggregates is 2, meaning there exists two large reverse micelles. After 14.5 ns, only 1 RM

exists in the system. From the microscopic information mentioned above, the process of di-CF4 self-assembly in scCO<sub>2</sub> can be speculated as three steps: (1) di-CF4 molecules aggregate and rapidly form several small RMs. (2) These small RMs (containing about 12 surfactant molecules) contact and merge into unstable rod-like RMs. (3) The rod-like RMs shrink and change into the stable spherical RMs.

### 3.2 The Reverse Micelle Structure

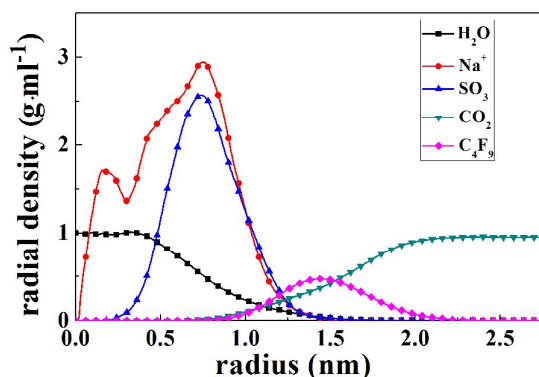


Fig. 3. Radial density profiles with respect to the center of mass of the RM core for different species in the water/di-CF4/scCO<sub>2</sub> RM system.

To characterize the microscopic structure of the RM, we calculated the radial density profiles with respect to the center of mass of the water core for various species including water molecules, Na<sup>+</sup>, headgroups(SO<sub>3</sub>), CO<sub>2</sub> molecules and the C atom at the end of the tailgroups(C<sub>4</sub>F<sub>9</sub>), shown in Fig. 3. The density of water in the interior of the RM approaches 1.0 g/cm<sup>3</sup> at the region from 0 to 0.5 nm, suggesting that a bulk water domain exists in the water/di-CF4/scCO<sub>2</sub> microemulsion system. Beyond 0.5 nm, the water density has an obvious decay due to the penetration of the CO<sub>2</sub> molecules and the hydrophobic tailgroups to the aqueous core. A bulk scCO<sub>2</sub> phase is also observed with the approximate density of 0.89 g/cm<sup>3</sup> at the region far from the interface between the tails and the scCO<sub>2</sub> phase, which is close to the experimental value of 0.84 g/cm<sup>3</sup> given by National Institute Standards and Technology (NIST) at the same temperature and pressure. The location of the Na<sup>+</sup> peak is at about 0.85 nm close to that of the SO<sub>3</sub> group, meaning that Na<sup>+</sup> cations accompanying with the SO<sub>3</sub> group are mainly near the interfacial region between the headgroups and the water phase. However, there are some Na<sup>+</sup> cations solvated in the water core, which is observed by the lower peak of Na<sup>+</sup> cations. Comparing the profiles of the tails of di-CF4 and the water molecules at the region from 0.8 nm to 1.25 nm, we find that the hydrophobic tails penetrate into the water core in the RM to some extent. It may be caused by the interactions between the strong polar F atoms and the water molecules. Comparing the profiles of the tails of

di-CF4 molecules and the CO<sub>2</sub> molecules at the region from 1.0 nm to 2.0 nm, we also observe that many CO<sub>2</sub> molecules penetrate into the di-CF4 monolayer. Consequently, the radial density profiles shown in Fig. 3 indicate four regions existing in the water/di-CF4/scCO<sub>2</sub> system: the aqueous core, the interfacial region between the SO<sub>3</sub> groups and the water phase, the interfacial region between the tailgroups and the scCO<sub>2</sub> phase, and the bulk scCO<sub>2</sub> phase. In addition, the profiles of the SO<sub>3</sub> groups and the tailgroups are symmetrical, implying that the RM is stable and spherical.

The radius of gyration,  $R_g$ , describing the distribution of the mass of atomic groups or molecules that constitute the aqueous core relative to its center of mass, is a good measure of the size of the reverse micelle.  $R_g$  is described by<sup>50</sup>

$$R_g^2 = \frac{\sum_i m_i (r_i - r_0)^2}{\sum_i m_i} \quad (2)$$

Where “ $i$ ” includes all surfactant atoms, cations, and water molecules in the RM region.  $m_i$  is the mass of atom  $i$  and  $r_i$  is the distance of atom  $i$  from the center of mass  $r_0$  of the aggregated core. Fig. 4 shows the time evolution of the radius of gyration during the last 2 ns run. It is observed that the radius of gyration for the water core is about 1.54 nm with a little fluctuation, which is in reasonable agreement with the experimental value of 1.9 nm measured by SANS experiments<sup>38</sup>. Moreover, the radii of gyration of the headgroups and the tailgroups are almost constant with values of 0.85 nm and 1.7 nm, respectively, revealing that the RM remains a spherical shape.

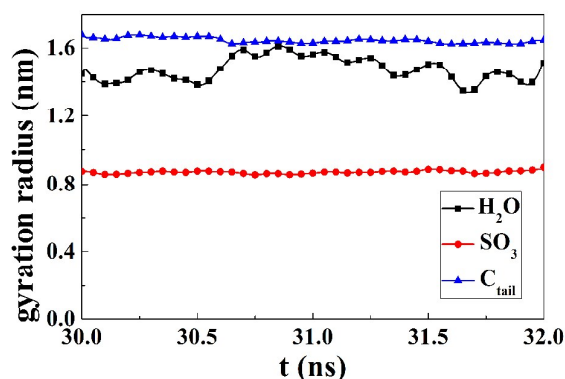


Fig. 4. The time evolution of the gyration radius during the last 2 ns run.

### 3.3 Hydrogen Bonds

The hydrogen bond (H-bond) is an important characteristic of the water molecules in the aqueous core of the RM, which has a significant effect on the stability of the RM. Note that the headgroups of di-CF<sub>4</sub> molecules contain oxygen atoms that are capable of forming hydrogen bonds with the water hydrogens. In addition, H-bonds also form among water molecules themselves. In this work, a hydrogen bond is defined to exist if the oxygen-oxygen distance is less than 3.5 Å and simultaneously the angle of hydrogen-oxygen-oxygen is less than 30°<sup>51</sup>. Fig. 5 shows several typical H-bonds in the RM. Fig. 5a shows the H-bond formed by one O atom in the headgroup and water molecules. Fig. 5b indicates the H-bond between two O atoms in the headgroup and the water molecules. However, we did not observe the H-bond simultaneously formed by water molecules and three O atoms in one headgroup. Fig. 5c illustrates that two headgroups, forming H-bonds with water molecules respectively, connect with each other through the H-bonds among their neighbour water molecules. Fig. 5d shows a similar structure to that in Fig. 5c. However, the difference is that there are two Na<sup>+</sup> between two headgroups in Fig. 5c. Comparing these two figures, we find that di-CF<sub>4</sub> molecules in Fig. 5d are more compact to cover the surface of the aqueous core, leading to a smaller packing area of the headgroup in the RM. The strong H-bonds weaken the electrostatic repulsion between headgroups and strongly constrain the moving range of di-CF<sub>4</sub> molecules, which are beneficial to stabilize the RM.

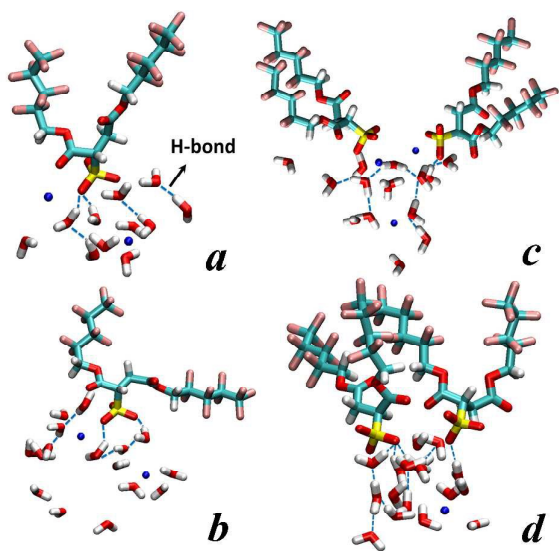


Fig. 5. H-bonds structure around the headgroups. Color code, blue: Na<sup>+</sup> ions, red: oxygen atoms, white: hydrogen atoms, watchet: carbon atoms, pink: fluorine atoms.

### 3.4 Salt Bridges

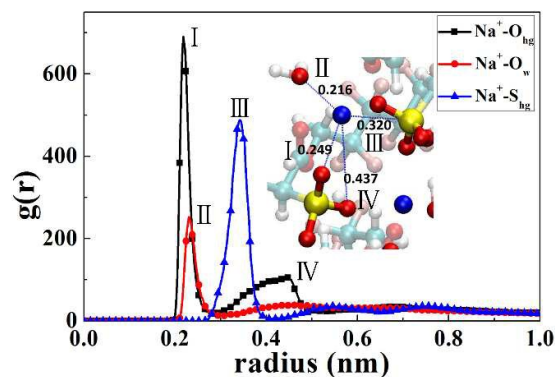


Fig. 6. Radial distribution function profiles for the [Na][di-CF<sub>4</sub>]-water pairs in system. 1 Black: Na<sup>+</sup>-O<sub>hg</sub> (oxygen in headgroups), 2 red: Na<sup>+</sup>-O<sub>w</sub> (oxygen in water), 3 blue: Na<sup>+</sup>-S<sub>hg</sub> (sulphur in headgroups).

To study the binding behaviour among the surfactant, water and ions, various site-site radial distribution functions (RDFs) for Na<sup>+</sup>-O<sub>hg</sub> (O atoms in headgroups), Na<sup>+</sup>-S<sub>hg</sub> (S atoms in headgroups) and Na<sup>+</sup>-O<sub>w</sub> (O atoms in water molecules) were calculated and shown in Fig. 6. The Na<sup>+</sup>-O<sub>hg</sub> RDF has a prominent first peak at 0.22 nm and a minimum at 0.28 nm, described by the structure I in the inset. The second peak is at 0.43 nm due to the remaining two O atoms in the headgroup, illustrated by the structure IV in the inset. The peak of the Na<sup>+</sup>-S<sub>hg</sub> RDF locates at 0.28 nm corresponding to the structure III in the inset. The results show that most of Na<sup>+</sup> are constrained near the negatively charged di-CF<sub>4</sub> headgroups. The Na<sup>+</sup>-O<sub>w</sub> RDF shows a distinct first peak at 0.23 nm corresponding to the structure II in the inset, indicating a distinct hydration shell there. A second hydration peak existing at 0.43 nm is also observed. These two hydration shells imply a strong structuring of water molecules around Na<sup>+</sup>.

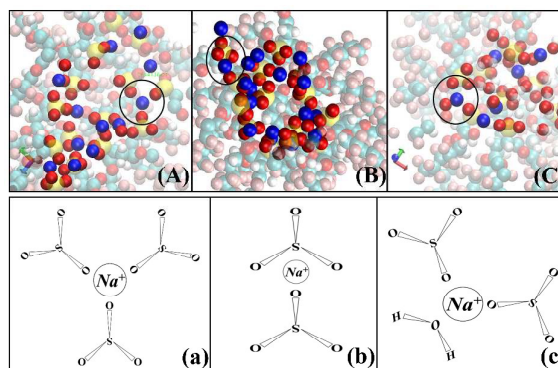


Fig. 7. Snapshots for the typical salt bridges in the RM. The color scheme: blue: Na<sup>+</sup>, red: oxygen atoms in headgroups, yellow: sulphur, water molecules are omitted, and the headgroups are highlighted for clarity. (a), (b) and (c) are the schematic diagrams for salt bridge styles in the RM.

From the above analysis of RDFs for Na<sup>+</sup>-headgroup and Na<sup>+</sup>-water, we find a prominent structure of Na<sup>+</sup> interacting with headgroups and water in the RM, which is illustrated by the inset in Fig. 6. The structure shows that Na<sup>+</sup> can combine with headgroups to stabilize the RM, which is called salt bridge. It is assumed that one Na<sup>+</sup> bridges two anionic headgroups or three if it resides within a distance 0.58 nm from two nearest-neighbour headgroup pairs.<sup>52</sup> According to the number of headgroups bridged by one Na<sup>+</sup>, three types of salt bridges are observed in the RM, shown in Fig. 7. Fig. 7(A) shows that Na<sup>+</sup> is shared by three O atoms in different headgroups. Fig. 7(B) shows that Na<sup>+</sup> is shared by two O atoms in one headgroup and one O atom in the other headgroup. Fig. 7(C) shows that Na<sup>+</sup> is shared by two O atoms in different headgroups and one O atom in a water molecule. Fig. 7 (a), (b) and (c) are the schematic diagrams for the salt bridges occurring in the RM. The formation of the salt bridge can shield the electrostatic repulsion<sup>53</sup> between polar components, and thus the monolayer of surfactants will be compact enough to stabilize the RM.

### 3.5 Surfactant Coverage

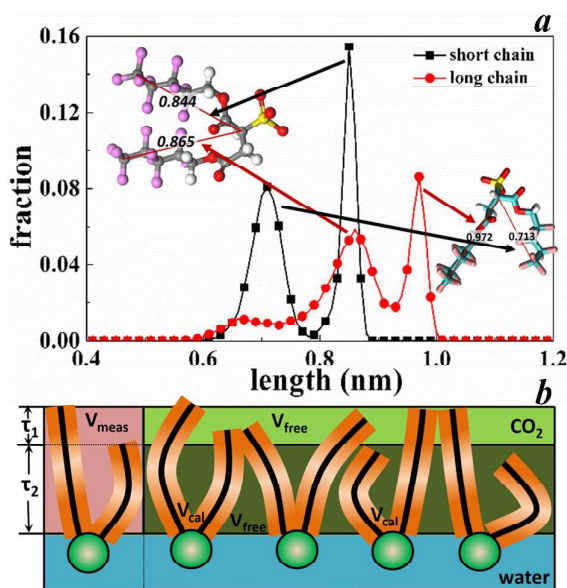


Fig. 8. a: The length fraction distribution of two tailgroups. The black line is the distribution of the short chain which is the C-COO-CH<sub>2</sub>-(CF<sub>2</sub>)<sub>3</sub>-CF<sub>3</sub> and the red line represent the long chain of the surfactants C-CH<sub>2</sub>-COO-CH<sub>2</sub>-(CF<sub>2</sub>)<sub>3</sub>-CF<sub>3</sub>. b: The surfactants monolayer schematic diagram according to the length distribution.

The chemical factors determining CO<sub>2</sub>-philicity is vital to design CO<sub>2</sub>-compatible surfactants in developing the practical applications of the dense CO<sub>2</sub>. The CO<sub>2</sub>-philicity of a given surfactant was predicted by the measurement of fractional

free volume (FFV) on the basis of previous studies<sup>17, 25, 26</sup>. However, the FFV approach has limitations in distinguishing between hydrocarbon and fluorocarbon surfactants. Recently, the relative surfactant coverage  $\Phi_{surf}$ , proposed to be a new predictive model for CO<sub>2</sub>-philic surfactant design, is expressed as

$$\Phi_{surf} = \frac{V_{cal}}{V_{meas}} \quad (2)$$

Where  $V_{cal}$  is the total physical volume of surfactant molecular fragment<sup>54, 55</sup>, and  $V_{meas}$  is the total volume occupied by a surfactant molecule at the water-CO<sub>2</sub> interface. In this work,  $\Phi_{surf}$  for the di-CF<sub>4</sub> molecule was calculated to be 0.788 lower than the experimental value of 0.970<sup>17</sup>. The calculation for  $\Phi_{surf}$  in detail was given in Electronic Supporting Information (ESI). The difference between them mainly results from the interface on which  $\Phi_{surf}$  was computed. Our result was obtained on the spherical monolayer in the RM while the experimental value of  $\Phi_{surf}$  was calculated on the planar monolayer. The high  $\Phi_{surf}$  indicates the high interfacial packing efficiency and therefore the enhancement in the CO<sub>2</sub>-philicity. On the other hand, the bend of the tailgroup also decreases  $V_{meas}$ , contributing to the increase in  $\Phi_{surf}$ .

To study the bend behaviour of the tailgroup, the probability distribution for the chain length of the tailgroup was calculated and plotted in Fig. 8a. Here, the chain length of the tailgroup is defined as the distance between the C atom at the end of the tail and the C atom bonding with the S atom, shown by the inset in Fig. 8a. It is observed that there are two prominent peaks for both the short chain (C-COO-CH<sub>2</sub>-(CF<sub>2</sub>)<sub>3</sub>-CF<sub>3</sub>) and the long chain (C-CH<sub>2</sub>-COO-CH<sub>2</sub>-(CF<sub>2</sub>)<sub>3</sub>-CF<sub>3</sub>) in the RM. The higher peak for the short chain locates at 0.85 nm corresponding to its length of 0.844 nm in the free di-CF<sub>4</sub> molecule. The lower peak occurs at 0.713 nm showing the bend of the short chain happens in the RM. The lower peak for the long chain locates at 0.87 nm corresponding to its length of 0.865 nm in the free di-CF<sub>4</sub> molecule. The higher peak occurs at 0.972 nm indicating the stretch of the long chain happens in the RM. For the purpose of visualization, the structure of the di-CF<sub>4</sub> molecule in the free state and that in the RM are depicted by the upper-left inset and the bottom-right inset, respectively. Thus, the interfacial region between the water phase and the CO<sub>2</sub> phase can be described by Fig. 8b. In the region  $\tau_1$ ,  $\Phi_{surf}$  obviously decreases and equals 0.346. In the region  $\tau_2$ ,  $\Phi_{surf}$  increases and equals 0.824. It implies that the bend of the short chain plays the dominant role in the formation of the RM for the water/di-CF<sub>4</sub>/scCO<sub>2</sub> system. The monolayer structure shown in Fig. 8b can efficiently segregate the CO<sub>2</sub> phase from the water phase. At the same time, it can enhance the interaction between the CO<sub>2</sub> molecules and the tailgroups due to the large bare CF group area in region  $\tau_1$ .

To explore the tailgroups bending behaviour, the average fraction of gauche defects in the system was calculated. In this work, a gauche defect is defined to exist if the dihedral is less than 60°. The dihedral involving a carboxyl linkage (H2C-C-O-CF2) in two chains are much different. The gauche fraction of the dihedral in short chain is 0.55 higher than that in the long chain of 0.35, indicating the short chain bends and the long chain stretches. Moreover, it also shows that the presence of the carboxyl linkages to the perfluorinated chain can increase the flexibility significantly<sup>56, 57</sup>, by which the chain bends or stretches to increase the surfactant interfacial packing efficiency.

#### 4. Conclusions

Molecular dynamics simulations were performed to study the self-assembly of the double-chain fluorocarbon surfactants, di-CF4, in scCO<sub>2</sub>. The stable and spherical RM with the radius of 1.7 nm is formed in the water/di-CF4/scCO<sub>2</sub> system, which is in well agreement with the experiments. The dynamics process and the number of the aggregates indicate that the self-assembly process could be speculated as three steps: (1) di-CF4 molecules aggregate and rapidly form several small RMs. (2) These small RMs (containing about 12 surfactant molecules) contact and merge into unstable rod-like RMs. (3) The rod-like RMs shrink and change into a stable spherical RMs. The hydrogen bonds between headgroups and water molecules, and the salt bridges among Na<sup>+</sup>, headgroups and water molecules are responsible for the tuning of di-CF4 molecules packing over the RM interface. This increases the surfactant coverage  $\Phi_{\text{surf}}$  and thus play a significant role in stabilizing the RM. The  $\Phi_{\text{surf}}$  on the spherical RM interface is 0.788 less than the experimental value of 0.970 on the planar micellar interface. The high  $\Phi_{\text{surf}}$  implying the high interfacial packing efficiency enhances the CO<sub>2</sub>-philicity for the di-CF4 molecule. The bend of the short chain (C-COO-CH2-(CF2)3-CF3) dominates the enhancement in the interfacial packing efficiency of the di-CF4 molecules, while the stretch of the long chain (C-CH2-COO-CH2-(CF2)3-CF3) decreases the  $\Phi_{\text{surf}}$ . The carboxyl linkage (H2C-C-O-CF2) to the perfluorinated chain mainly results in the bend or stretch of the tail chains, which significantly increases the flexibility of the tailgroups.

This work shows the intrinsic correlation between salt bridges, surfactant coverage and the RM, with self-aggregation behavior in scCO<sub>2</sub>, which elucidates the fundamental mechanism of the self-assembly. The design of specific optimized architectures to boost the efficacy of CO<sub>2</sub> solvency enhancement can be envisaged by controlling the counterions, the carboxyl linkage type in tailgroup and the branched degree of the tail. The results will be helpful to design CO<sub>2</sub>-philic hybrid surfactant with low fluorine content, and reduce the guesswork in finding CO<sub>2</sub>-philic compound.

#### Acknowledgements

This work was financially supported by the Petro China Innovation Foundation (2014D-5006-0211), the National Natural Science Foundation of China (U1262202), the Fundamental Research Funds for the Central Universities (14CX05022A, 15CX08003A), the National Basic Research Program of China (2014CB239204, 2015CB250904), and the Shandong Provincial Natural Science Foundation, China (ZR2014EEM035). The Research Council of Norway, Det Norske Oljeselskap ASA, and Wintershall Norge AS are acknowledged for funding support via WINPA project (Nano2021 and Petromaks2 234626/O70).

#### Notes and references

1. C. James and J. Eastoe, *Curr. Opin. Colloid Interface Sci.*, 2013, **18**, 40-46.
2. K. Trickett, D. Xing, R. Enick, J. Eastoe, M. J. Hollamby, K. J. Mutch, S. E. Rogers, R. K. Heenan and D. C. Steytler, *Langmuir*, 2009, **26**, 83-88.
3. R. Ullah, M. Atilhan, B. Anaya, M. Khraisheh, G. García, A. ElKhattat, M. Tariq and S. Aparicio, *Phys. Chem. Chem. Phys.*, 2015, **17**, 20941-20960.
4. C. Yan, M. Sagisaka, S. E. Rogers, G. Hazell, J. Peach and J. Eastoe, *Langmuir*, 2016, **32**, 1421-1428.
5. B. Wu, X. Yang, Z. Xu and Z. Xu, *Colloids Surf., A*, 2010, **367**, 148-154.
6. S. Salaniwal, S. Cui, P. Cummings and H. Cochran, *Langmuir*, 1999, **15**, 5188-5192.
7. E. Goetheer, M. Vorstman and J. Keurentjes, *Chem. Eng. Sci.*, 1999, **54**, 1589-1596.
8. F. Rezaei, Y. Yamini, H. Asiabi, S. Seidi and M. Rezazadeh, *J. Supercrit. Fluids*, 2016, **107**, 392-399.
9. K. Trickett, D. Xing, R. Enick, J. Eastoe, M. J. Hollamby, K. J. Mutch, S. E. Rogers, R. K. Heenan and D. C. Steytler, *Langmuir*, 2010, **26**, 83-88.
10. J. Eastoe, A. Downer, A. Paul, D. C. Steytler, E. Rumsey, J. Penfold and R. K. Heenan, *Phys. Chem. Chem. Phys.*, 2000, **2**, 5235-5242.
11. M. Sagisaka, S. Ono, C. James, A. Yoshizawa, A. Mohamed, F. Guittard, S. E. Rogers, R. K. Heenan, C. Yan and J. Eastoe, *Langmuir*, 2015, **31**, 7479-7487.
12. M. Sagisaka, S. Iwama, A. Yoshizawa, A. Mohamed, S. Cummings and J. Eastoe, *Langmuir*, 2012, **28**, 10988-10996.
13. M. Sagisaka, S. Iwama, S. Ono, A. Yoshizawa, A. Mohamed, S. Cummings, C. Yan, C. James, S. E. Rogers, R. K. Heenan and J. Eastoe, *Langmuir*, 2013, **29**, 7618-7628.
14. C. James, M. H. Hatzopoulos, C. Yan, G. N. Smith, S. Alexander, S. E. Rogers and J. Eastoe, *Langmuir*, 2014, **30**, 96-102.
15. A. Mohamed, T. Ardyani, S. A. Bakar, M. Sagisaka, S. Ono, T. Narumi, M. Kubota, P. Brown and J. Eastoe, *J. Supercrit. Fluids*, 2016 **116**, 158-164.
16. M. Sagisaka, S. Yoda, Y. Takebayashi, K. Otake, B. Kitiyanan, Y. Kondo, N. Yoshino, K. Takebayashi, H. Sakai and M. Abe, *Langmuir*, 2003, **19**, 220-225.
17. A. Mohamed, M. Sagisaka, F. Guittard, S. Cummings, A. Paul, S. E. Rogers, R. K. Heenan, R. Dyer and J. Eastoe, *Langmuir*, 2011, **27**, 10562-10569.
18. K. Harrison, J. Goveas, K. P. Johnston and E. A. O'Rear III, *Langmuir*, 1994, **10**, 3536-3541.
19. S. Cummings, D. Xing, R. Enick, S. Rogers, R. Heenan, I. Grillo and

- J. Eastoe, *Soft Matter*, 2012, **8**, 7044-7055.
20. J. Eastoe, C. Yan and A. Mohamed, *Curr. Opin. Colloid Interface Sci.*, 2012, **17**, 266-273.
21. S. Zhuo, Y. Huang, C. Peng, H. Liu, Y. Hu and J. Jiang, *J. Phys. Chem. B*, 2010, **114**, 6344-6349.
22. L. Lu and M. L. Berkowitz, *J. Am. Chem. Soc.*, 2004, **126**, 10254-10255.
23. M. Bey Tamsamani, M. Maeck, I. El Hassani and H. D. Hurwitz, *J. Phys. Chem. B*, 1998, **102**, 3335-3340.
24. J. Faeder, M. V. Albert and B. M. Ladanyi, *Langmuir*, 2003, **19**, 2514-2520.
25. V. H. Dalvi, V. Srinivasan and P. J. Rossky, *J. Phys. Chem. C*, 2010, **114**, 15553-15561.
26. M. T. Stone, S. R. da Rocha, P. J. Rossky and K. P. Johnston, *J. Phys. Chem. B*, 2003, **107**, 10185-10192.
27. M. T. Stone, P. G. Smith, S. R. da Rocha, P. J. Rossky and K. P. Johnston, *J. Phys. Chem. B*, 2004, **108**, 1962-1966.
28. V. H. Dalvi, V. Srinivasan and P. J. Rossky, *J. Phys. Chem. C*, 2010, **114**, 15562-15573.
29. N. Sapay and D. P. Tieleman, *J. Comput. Chem*, 2011, **32**, 1400-1410.
30. A. D. MacKerell, B. Brooks, C. L. Brooks, L. Nilsson, B. Roux, Y. Won and M. Karplus, *Encyclopedia of computational chemistry*, 1998.
31. K. Vanommeslaeghe, E. Hatcher, C. Acharya, S. Kundu, S. Zhong, J. Shim, E. Darian, O. Guvench, P. Lopes and I. Vorobyov, *J. Comput. Chem*, 2010, **31**, 671-690.
32. V. Zoete, M. A. Cuendet, A. Grosdidier and O. Michielin, *J. Comput. Chem*, 2011, **32**, 2359-2368.
33. P. Mark and L. Nilsson, *J. Phys. Chem. A*, 2001, **105**, 9954-9960.
34. J. G. Harris and K. H. Yung, *J. Phys. Chem.*, 1995, **99**, 12021-12024.
35. A. White, *Intermolecular potentials of mixed systems: Testing the Lorentz-Berthelot mixing rules with Ab initio calculations*, DTIC Document, 2000.
36. A. K. Al - Matar and D. A. Rockstraw, *J. Comput. Chem*, 2004, **25**, 660-668.
37. L. Martínez, R. Andrade, E. G. Birgin and J. M. Martínez, *J. Comput. Chem*, 2009, **30**, 2157-2164.
38. J. Eastoe, A. Paul, A. Downer, D. C. Steytler and E. Rumsey, *Langmuir*, 2002, **18**, 3014-3017.
39. S. Pronk, S. Páll, R. Schulz, P. Larsson, P. Bjelkmar, R. Apostolov, M. R. Shirts, J. C. Smith, P. M. Kasson and D. van der Spoel, *Bioinformatics*, 2013, **29**, 845-854.
40. W. Humphrey, A. Dalke and K. Schulten, *J. Mol. Graphics*, 1996, **14**, 33-38.
41. D. J. Evans and B. L. Holian, *J. Chem. Phys.*, 1985, **83**, 4069-4074.
42. G. J. Martyna, M. L. Klein and M. Tuckerman, *J. Chem. Phys.*, 1992, **97**, 2635-2643.
43. L. Verlet, *Phys. Rev.*, 1967, **159**, 98.
44. T. Darden, D. York and L. Pedersen, *J. Chem. Phys.*, 1993, **98**, 10089-10092.
45. L. V. Zhigilei and B. J. Garrison, *Appl. Phys. Lett.*, 1997, **71**, 551-553.
46. S. Salaniwal, S. Cui, H. Cochran and P. Cummings, *Langmuir*, 2001, **17**, 1773-1783.
47. H. Gochman-Hecht and H. Bianco-Peled, *J. Colloid Interface Sci.*, 2005, **288**, 230-237.
48. G. Cassin, J. Badiali and M. Pileni, *J. Phys. Chem.*, 1995, **99**, 12941-12946.
49. J. C. Gower and G. Ross, *Applied statistics*, 1969, **18** 54-64.
50. M. K. Shimamura and T. Deguchi, *Phys. Rev. E*, 2002, **65**, 051802.
51. A. Luzar and D. Chandler, *J. Chem. Phys.*, 1993, **98**, 8160-8173.
52. H. Yan, X.-L. Guo, S.-L. Yuan and C.-B. Liu, *Langmuir*, 2011, **27**, 5762-5771.
53. J. Busalmen and S. De Sanchez, *Appl. Environ. Microbiol.*, 2001, **67**, 3188-3194.
54. L. Zhang, Z. Liu, T. Ren, P. Wu, J.-W. Shen, W. Zhang and X. Wang, *Langmuir*, 2014, **30**, 13815-13822.
55. S. S. Berr and R. R. Jones, *J. Phys. Chem.*, 1989, **93**, 2555-2558.
56. G. D. Smith, R. L. Jaffe and D. Y. Yoon, *Macromolecules*, 1995, **28**, 5804-5810.
57. S. R. da Rocha, K. P. Johnston and P. J. Rossky, *J. Phys. Chem. B*, 2002, **106**, 13250-13261.